12-1-2009

Precipitate Redistribution During Creep of Alloy 617

Scott Schlegel
Boise State University

Sharla Hopkins
Boise State University

E. Young
Boise State University

James Cole
Idaho National Laboratory

Thomas Lillo
Idaho National Laboratory

See next page for additional authors

Authors
Scott Schlegel, Sharla Hopkins, E. Young, James Cole, Thomas Lillo, and Megan Frary

Precipitate Redistribution during Creep of Alloy 617

S. Schlegel*, S. Hopkins*, E. Young*, J. Cole†, T. Lillo†, M. Frary*

* Materials Science and Engineering, Boise State University, Boise, ID

† Idaho National Laboratory, Idaho Falls, ID

Abstract

Nickel-based superalloys are being considered for applications within advanced nuclear power generation systems due to their high temperature strength and corrosion resistance. Alloy 617, a candidate for use in heat exchangers, derives its strength from both solid solution strengthening and the precipitation of carbide particles. However, during creep, carbides that are supposed to retard grain boundary motion are found to dissolve and re-precipitate on boundaries in tension. To quantify the redistribution, we have used electron backscatter diffraction and energy dispersive spectroscopy to analyze the microstructure of 617 after creep testing at 900 and 1000°C. The data were analyzed with respect to location of the carbides (e.g., intergranular vs. intragranular), grain boundary character, and precipitate type (i.e., Cr-rich or Mo-rich). We find that grain boundary character is the most important factor in carbide distribution; some evidence of preferential distribution to boundaries in tension is also observed at higher applied stresses. Finally, the results suggest that the observed redistribution is due to the migration of carbides to the boundaries and not the migration of boundaries to the precipitates.

1. Introduction

Advanced energy systems require metallic materials that have a combination of resistance to deformation at high temperature, resistance to environmental degradation in the operating environment, and stability of properties for long periods of time. For example, the Next Generation Nuclear Plant may require alloys to operate in oxidizing or mildly carburizing impure helium gas at temperatures above 900ºC for a period of more than 60 years. A similar set of property requirements are likely for materials in systems using thermo-chemical production of hydrogen or in ultra super-critical steam plants.

The required combination of creep resistance, corrosion resistance and stability restricts the choices of alloys for high temperature energy systems to high-chromium, nickel-based solid solution alloys with relatively large and stable grain sizes. In nickel-based alloy 617, the focus of the present study, solution strengthening is imparted primarily by Co and Mo, while oxidation resistance is provided predominantly by Cr and Al. Under oxidizing conditions, Cr forms a dense oxide scale that protects the alloy from significant environmental degradation.[1] In addition, the grain structure of 617 is stabilized after long-term exposure to elevated temperature by the formation of both intergranular and intragranular carbides with composition $Cr_{23}C_6$ or Mo_6C. The presence of carbides on the grain boundaries prevents boundary migration and contributes to creep resistance.[2] The Cr-rich carbides are thought to reside primarily on the grain boundaries, while the Mo-rich boundaries are usually found within the grains.[2-7] Both intragranular and intergranular carbides are believed to affect the mechanical,[8, 9] creep,[2, 6, 7] and fatigue [7, 10] properties of the alloy.

During prolonged exposure at elevated temperatures, evolution of the precipitate distribution is possible. For example, in their study of prolonged aging of alloy 617 for times of ~20,000 and 50,000 h at 871°C, Wu *et al.* [11] found that the fine M_6C precipitates dissolved, while coarse M_6C remained both at the grain boundaries and in the grain interiors. Coarse (μm-sized) $M_{23}C_6$ precipitates also formed at the boundaries after extended aging.[11] If the material is simultaneously exposed to high temperature and stress, e.g., in a creep deformation environment, some circumstances lead to the migration of the Cr-rich carbides to the grain boundaries under tensile stress, while the Mo_6C carbides apparently go into solution.[2] During this process, grain boundaries that are in compression become denuded of carbides and are then free to migrate. It has been suggested that the resulting grain growth leads to rapid material failure.[2] Kihara *et al.* proposed a mechanism for the precipitate redistribution wherein the migration occurs by dissolution, diffusion, and re-precipitation of the carbides from regions in compression to regions in tension.[2] The difference in stability of the carbides in compressive versus tensile environments is believed to be the driving force for the re-distribution.[2] In Ref. [2], the majority of the grain boundary precipitates were found to be Cr-rich ($M_{23}C_6$) carbides, and the higher fraction of Cr-rich carbides on the grain boundaries was suggested to be due to the higher diffusivity of chromium than molybdenum in nickel-based alloys. Prior to creep, the Mo-rich carbides were found primarily within the grains. [2] Therefore, as the intragranular carbides went into solution, the rate of diffusion of solute chromium atoms was greater than that of the molybdenum atoms, and as a result, the chromium carbides precipitated in higher numbers and subsequently grew at higher rates than the Mo-rich carbides. During elevated temperature low-cycle fatigue testing, Smith and Yates found that the Mo-rich carbides tended to be more

resistant to dissolution than the Cr-rich $M_{23}C_6$ carbides.[10] In related work, He *et al.* performed tensile creep tests at 800°C on the Ni-based superalloy M963 and determined that the precipitation of the Cr-rich $M_{23}C_6$ phase was strongly dependent on both stress and temperature.[12]

The microstructure of creep-tested alloy 617 is shown in Figure 1 where it is apparent that the majority of carbides are on boundaries that were subjected to tensile stress (i.e., normal to the stress axis). Although carbide redistribution has been observed in previous studies, there is not a clear understanding of the phenomenon or the mechanism responsible. The temperature dependence and the kinetics of the redistribution of the carbides have not been studied in detail; neither is it known with any certainty if the carbide redistribution is actually stress- or strain-assisted. It is also apparent from Figure 1 that not all boundaries normal to the stress axis are decorated with carbides; twin boundaries appear to have a low density of carbides.

In order to understand the role grain boundary character plays in precipitate redistribution, an appropriate boundary classification scheme must be defined. The binary classification of grain boundaries as either special or general has been used to correlate many observed properties to grain boundary structure.[13-15] In this framework, general boundaries are those exhibiting undesirable properties (e.g., susceptibility to cracking or corrosion) and have been shown to correspond to boundary structures with low atomic matching.[13-15] In contrast, special grain boundaries are those with desirable properties (e.g., resistance to cracking or corrosion), which have been correlated to boundary structures with a high degree of atomic matching.[13-15] Grain boundaries are typically classified on the basis of their structure as either low-angle (those with misorientations up to 15°) or high-angle (those with misorientations greater than 15°).[16] Low-angle boundaries generally exhibit lower interfacial energy as compared to high-angle boundaries as a result of the differences in atomic mismatch.[16] As a result, low-angle boundaries are classified as "special" while high-angle boundaries are labeled "general". However, certain high-angle grain boundaries have been found to exhibit energies or properties comparable to low-angle grain boundaries.[17, 18] These low-energy high-angle grain boundaries exhibit a high degree of atomic matching, which can be described using the coincidence site lattice (CSL) model, and are also typically classified as "special" boundaries.[13-15] CSL boundaries may be characterized by the coincidence index Σ, which gives the reciprocal density of coincidence sites. While it is common to define all CSL boundaries with $\Sigma \leq 29$ as special, not all of these demonstrate special properties or low energy, characteristics found most commonly in twin-related boundaries (i.e., those with $\Sigma 3^n$). The classification of a grain boundary as either special or general can be accomplished by measuring the misorientation between adjacent grains using electron backscatter diffraction.

Grain boundary character has been shown to influence both carbide precipitation [4, 5, 19, 20] and thermal stability of the microstructure.[21-24] Studies of nickel-based superalloys have shown that the precipitation of grain boundary carbides is affected by grain boundary type. Lim *et al.* found coarse and irregular Cr-rich carbides ($M_{23}C_6$) distributed on general grain boundaries in Inconel 690.[4] Conversely, the authors observed that along low-Σ CSL grain boundaries, the carbides were fine and densely distributed, with the exception being coherent twins ($\Sigma 3$), which were devoid of any carbides.[4] In a related study of carbide precipitates in a ternary nickel alloy, Liu *et al.* observed that carbides on low-Σ CSL boundaries tended to be smaller and more closely

spaced than the carbides found on the general grain boundaries.[5] Both studies concluded that precipitation of the intergranular carbides was suppressed on low-Σ CSL boundaries, as compared to the general high-angle boundaries, based on the influence of grain boundary energy. Previous studies of aluminum and copper alloys have also shown that precipitation is affected the grain boundary character.[5, 20]

One of the objectives of the present work is to quantify the effect of grain boundary character on precipitate redistribution, accounting for precipitate type, precipitate density (number of precipitates per grain boundary length), grain boundary type and the angle between the grain boundary trace and the applied stress axis. Two previous studies [19, 20] have used a related approach in quantifying the average number density of precipitates on grain boundaries. Li *et al.* [20] used TEM to measure the number density of precipitates in an Al alloy as a function of aging time, but did not differentiate on the basis of grain boundary character. Hong *et al.* [19] studied carbide precipitation in stainless steel and correlated the carbide number density with grain boundary type (Σ3, Σ5 through 27, and random boundaries). In the present investigation of creep deformed alloy 617, we not only measure carbide density, but also quantify the precipitate distribution with respect to grain boundary character using several other novel metrics. In a related paper in this issue by Lillo *et al.*[25], creep voids are characterized using similar metrics. Here, microstructural characterization is performed using simultaneous electron backscattered diffraction (EBSD) and energy dispersive spectroscopy (EDS) which provide quantitative data on the type and location of both precipitates and grain boundaries. Analysis of these data give insight to the preferential precipitate distribution and elucidate the role that both applied load and temperature play in the redistribution process.

2. Experimental Procedures

2.1. Materials and Testing Procedures

The material used in the present study was Inconel 617 (UNS N06617) from Special Metals Corporation (New Hartford, NY). The composition of the as-received material is given in Table 1. Creep testing was performed on specimens in the as-received condition (Figure 2) with geometry as defined by ASTM Standard E 139-06. The gauge length was 16.6 mm and the gauge diameter 4.2 mm. Specimens were cut from a 1.9 cm thick plate such that the long axis of the creep specimen was in the plane of the plate. High temperature creep tests were carried out using an Applied Test Systems Lever Arm Tester (Series 2410) with the parameters given in Table 2. The temperature was monitored with a K type thermocouple and controlled to within ±3°C of the target test temperature. Creep displacement was monitored with an LVDT during the test, but only to determine when the test should be terminated. The actual creep strain was determined by measuring the increase in sample length after the test was completed and the sample cooled to room temperature (cooling occurred under load).

After testing, both grip ends and gauge sections were cut and mounted for metallographic examination. The grip ends are assumed to have seen essentially no stress but to have spent the same amount of time at elevated temperature as their corresponding gauge sections. Characterization of both areas (with and without applied stress) will allow conclusions to be drawn about the effects of stress and temperatures separately. In what follows, the grip end

sections will be referred to as "annealed" and gauge sections as "creep deformed." Both grip and gauge sections were mounted in a configuration that provides a plane of view parallel to the specimen axis. Standard metallographic preparation was used and specimens were etched with a bromine solution (1% bromine and methanol) for 15 to 45 s to reveal the grain structure for subsequent characterization.

Microstructural characterization of both the creep tested and annealed sections was performed using a Philips XL30 ESEM with an EDAX/TSL Digiview III electron backscatter diffraction (EBSD) system and an EDAX/TSL Pegasus energy dispersive spectroscopy (EDS) detector. The EBSD/EDS data collection used an accelerating voltage of 20 to 30 kV and a step size of 0.1 to 0.8 μm with a hexagonal grid. In EBSD, all points whose orientations differ by less than 5° from their neighbors are considered to be in the same grain. Prior to analysis, EBSD data were subjected to the grain confidence index standardization cleanup method with a grain tolerance angle of 5° and a minimum grain size of two pixels. In addition, two iterations of the neighbor orientation correlation cleanup method were applied with a grain tolerance angle of 5°, minimum confidence index of 0, and cleanup level of 3. Initially, scan areas were typically less than 100×10^3 μm^2. While this area provided reasonable statistics for precipitate locations, it was often insufficient to show quantitative evidence of precipitate redistribution. Therefore, subsequent data sets were collected over areas typically greater than 200×10^3 μm^2. In what follows, data sets collected in each manner will be referred to as "small area scans" and "large area scans."

To investigate the microstructural stability in the thermomechanically-processed materials, the evolution of the grain boundary character distribution by length fraction was determined using the TSL OIM™ Analysis software's built-in capabilities. The Brandon criterion was applied in the analysis of CSL grain boundary character, where the allowable deviation from exact CSL misorientations is given as $\theta \leq 15\ \Sigma^{-1/2}$.[26] The resulting distribution provided the fraction of grain boundaries by length.

2.2. Analysis of Precipitate Distribution

The task of quantifying the carbide precipitate distribution in the creep tested specimens was undertaken by analyzing the EBSD/EDS data from the creep specimens using TSL OIM™ Analysis and ImageJ. The carbide precipitates were classified as either Cr-rich or Mo-rich using the EDS data to create concentration maps. The steps for the analysis are: (i) cleaning the data via the cleanup methods described previously, (ii) creating maps that revealed the grain boundaries and precipitates denoted by type (e.g., Figure 1), (iii) exporting the maps as JPEG images, and (iv) using ImageJ software to determine the grain boundary length, precipitate length, and grain boundary trace-angle relative to the creep stress axis.

The precipitate distribution was characterized using two methods. The first method focused on the precipitates, wherein the type, location, and number of precipitates were established (e.g., the number of intragranular Cr-rich carbides or the number of intergranular Mo-rich carbides). The second method evaluated each grain boundary in terms of its type, length, trace-angle relative to the creep stress axis, presence of precipitates, and the length of grain boundary occupied by precipitates. Through these two methods of microstructural

analysis, the precipitate distribution was quantified such that the location and number of all precipitates were determined, as well as the grain boundary character including trace-angle relative to the creep test stress axis and presence of precipitates.

Finally, we note that the analysis presented here is limited to carbides that can be detected by the combination of EBSD and EDS; in other words, only carbides greater than about 500 nm in diameter. While this may exclude many smaller precipitates, the analysis nevertheless can provide insight into the role of boundary character on the behavior of many of the carbides.

3. Results

3.1. Grain Size and Grain Boundary Character Distribution

Characterization of the as-received and creep-tested specimens was performed using simultaneous EBSD and EDS on randomly chosen areas. An example of a map resulting from the analysis is shown in Figure 1; grain boundaries are colored by type (special boundaries are red, general are black) and elemental information is shown as regions of blue and green, which correlate to high concentrations of Cr or Mo, respectively. The microstructure of the as-received material is shown in Figure 2. The horizontal direction in the image is parallel to the specimen and stress axis. The material is found to have a bimodal grain size distribution and bands of finer grains are found parallel to the specimen axis. During processing of the 617 plate, carbide particles are expected to spread out in planes parallel to the plane of the plate. In the as-received material (Fig. 2), the carbide precipitates that are present are aligned parallel to the specimen axis; quantitative analysis has confirmed this. In the as-received material, the preferential alignment likely results from the wrought processing of the plate. For a number of specimens, including the as-received material, some precipitate banding was observed where clusters of Mo- and Cr-rich precipitates formed bands parallel to the creep stress axis. In the analysis performed here, clusters of precipitates are not included and only individual precipitate particles are analyzed.

A summary of the results from the precipitate analysis including area of the specimen analyzed, mean grain size, grain boundary character distribution (GBCD), and number of precipitates and grain boundaries analyzed is given in Table 3. The standard deviation of the grain size distribution is on the order of the measured grain size. Differences between the small area scans and large area scans, both in terms of area and number of precipitates and boundaries, can be observed. The areas analyzed ranged from 16,200 to 320,100 μm^2, the number of precipitates from 39 (as-received) to 637, and the number of grain boundaries from 220 to 1340. As the grain size data show, there is little evidence of grain growth during high temperature exposure either with or without stress present. In some specimens, the grain size is smaller than in the as-received materials. This is likely due to the small scan area which was probably acquired from one of the fine-grained regions. In Table 3, the GBCD for each specimen is given as the length fraction of general high-angle (HA), low-angle (LA), and other low-Σ CSL boundaries ($\Sigma \leq 29$). The error associated with the measurement of grain boundary character is about 0.03. In most cases, 80 to 90% of the CSL boundaries are $\Sigma 3$ boundaries. The GBCDs did not show much variation between the creep deformed and annealed specimens; in other words, applied stress did not change the distribution of boundary types. However, those specimens that

were exposed to higher temperature (i.e., 1000°C vs. 900°C) did show an increase in the fraction of low-angle and other special boundaries.

3.2. Carbide Precipitate Analysis

The carbide distribution was initially characterized by the number of carbides (either Cr- or Mo-rich) that were located in the grains or on the grain boundaries (Figure 3). The results show that, in general, creep deformation at 900°C leads an increase in the fraction of precipitates on grain boundaries at the expense of precipitates within the grains as compared to the annealed specimens. This is evident in Figure 3 where the top two areas of each column (corresponding to precipitates on grain boundaries) increased when comparing annealed ($\sigma = 0$) to creep deformed ($\sigma > 0$) sections within a specimen set. The increase in the fraction of precipitates on grain boundaries was primarily due to an increase in the fraction of Mo-rich carbides on grain boundaries from grip to gauge sections; the Cr-rich carbides on boundaries did not have the same increase. For most of the specimens tested at 1000°C, there was little change in the distribution of precipitates by location (in grain vs. on boundaries), with the exception of the specimen tested at 1000°C and the highest stress, and no systematic changes in the location of either type of precipitate.

3.3. The Effect of Triple Junction Distribution on Carbide Precipitate Distribution

To determine if preferential precipitation occurred at certain triple junction types, the triple junction distribution (TJD) and the number of precipitates at the triple junctions were determined. The fraction of triple junctions with carbide precipitates *T(i,j)* is defined as:

$$T(i, j) = \frac{J_{i,j}}{N_j} \qquad (1)$$

where *i* is the type of precipitate (Cr-rich or Mo-rich), *j* is the number of special boundaries at the triple junction (0, 1, 2 or 3), N_j is the total number of triple junctions of type *j* in the scan area, and $J_{i,j}$ is the number of triple junctions of type *j* with precipitates of type *i*. Dividing by N_j thus takes into account the triple junction distribution in the microstructure. In most of the specimens, between 55 and 70% of the triple junctions were J_1 junctions (one special boundary and two general boundaries) and between 10 and 23% were J_2 junctions (two special boundaries and one general boundary). The results are presented in Figure 4 for representative data sets and show that, in general, triple junctions are more often populated by Mo-rich carbides than Cr-rich carbides. In addition, the grip sections of specimens tested at 1000°C show very high populations of carbides at the J_0 junctions (three general boundaries), while the J_0 junctions in the corresponding creep deformed specimens show lower carbide populations. In most cases, J_2 triple junctions are more likely to be populated by carbides than are J_1 and J_3 junctions; an explanation for this phenomena is presented in the discussion section.

3.4. The Effect of Grain Boundary Trace-Angle on Carbide Precipitate Distribution

Although Figure 3 showed the fraction of precipitates on grain boundaries, it provided no information about how the trace-angle of the boundary relative to the stress axis affected precipitate distribution. To this end, the presence or absence of carbide precipitates and grain boundary orientation relative to the creep stress axis were determined for each grain boundary in each data set. The distribution of grain boundaries with respect to the trace-angle relative to the creep stress axis was determined to ensure that the boundaries were uniformly distributed; the fraction of grain boundaries at each angular range was found to be relatively constant across the range of grain boundary angles. To determine whether the carbides preferentially precipitate on grain boundaries that experienced tensile stress versus compressive stress (i.e., if more precipitates are found on grain boundaries aligned closer to 90° from the stress axis), the fraction of grain boundaries with carbide precipitates $f(i,\theta)$ was determined as a function of boundary trace-angle as:

$$f(i,\theta) = \frac{B_{i,\theta}}{N_{\theta}} \tag{2}$$

where i is the precipitate type (Cr-rich, Mo-rich, or both types), θ is the trace-angle of the grain boundary with respect to the stress axis (in 10° increments), $B_{i,\theta}$ is the number of boundaries with angle θ and precipitates of type i, and N_θ is the total number of grain boundaries in that angular range. The results of this analysis are presented in Figure 5 for a subset of the specimens (in the interest of space). The graphs in the left column correspond to the annealed specimen from each pair. In these plots, the distribution of precipitates shows little correlation to the boundary trace-angle. As these specimens had essentially no applied stress to bias the diffusion of precipitate species along the grain boundaries or through the grain interiors, this result is expected. The graphs in the right column show the distribution of precipitates by boundary trace-angle for the creep deformed specimens. The top graph (900°C, 35 MPa) shows that the boundaries were very heavily decorated with precipitates after creep deformation. No other specimen showed nearly as many boundaries decorated with precipitates. However, this specimen had almost the smallest scan area and its possible that a very precipitate-rich region was analyzed. The distribution of precipitates for the 900°C, 35 MPa specimen indicates a shift toward boundaries in tension (i.e., boundaries whose trace-angles are nearer 90° are more likely to be populated by precipitates). The remaining three rows in Figure 5 correspond to specimens tested at 1000°C at increasing stresses and each corresponds to a large scan area. In the creep deformed specimens, the data indicate that an increase in stress may lead to a more pronounced shift in the distribution of precipitates to boundaries in tension (i.e., the trend is strongest for the 1000°C, 30 MPa specimen). In this work, we have found that the larger scan area may be necessary in order to quantitatively capture what can be qualitatively determined from a micrograph.

3.5. The Effect of Grain Boundary Character on Carbide Precipitate Distribution

In Figure 3, precipitate location was classified without regard to grain boundary character which may also play a role in the distribution of carbides; this was investigated by determining the fraction of carbide precipitates found on each type of grain boundary, $y(i,b)$, as:

$$y(i,b) = \frac{P_{i,b}}{N_{PPT}} \quad (3)$$

where i is the precipitate type (Cr-rich or Mo-rich), b is the type of grain boundary (low-angle, CSL ($\Sigma \leq 29$), or general), $P_{i,b}$ is the number of precipitates of type i on grain boundaries of type b, and N_{PPT} is the total number of precipitates analyzed that were on grain boundaries. Figure 6 shows the distribution of precipitates for each specimen with respect to grain boundary type. The fraction of precipitates on the general boundaries is represented by the two top-most segments; in nearly all specimens, the majority of precipitates were found on general boundaries, with the exceptions being the as-received and 1000°C, 18.6 MPa specimens. The fraction of precipitates found on low-angle grain boundaries was small in most specimens. At 900°C, no strong trend is observed when comparing the annealed ($\sigma = 0$) to creep deformed ($\sigma > 0$) sections. However, at 1000°C, a higher stress tends to lead to a bigger shift in precipitates onto the general boundaries. In Figure 6, a white circle is also plotted for each data set which corresponds to the fraction of special boundaries (low-angle and CSL). If precipitates were distributed equally among the boundaries present, the fraction of both Cr- and Mo-rich precipitates on the low-angle and other CSL boundaries (i.e., the four lower segments of each column) should have the same value as the special fraction. However, this is the case only in the as-received material. In general, the fraction of precipitates on the special boundaries is far lower than the special boundary fraction, which indicates that special boundaries are far less likely to be decorated with precipitates than are the general boundaries.

Figure 6 showed the type of grain boundaries that were populated by precipitates (i.e., which grain boundary types are the Mo-rich precipitates occupying). Another approach to determine the effect of grain boundary character on the distribution of carbides involves focusing on which precipitates are on the grain boundaries (i.e., which precipitates are found on the general grain boundaries). The length fraction of each grain boundary covered by carbide precipitates, $g(b,p,i)$, as a function of boundary type is determined as:

$$g(b,p,i) = \frac{B_{b,p,i}}{N_b} \quad (4)$$

where b is the type of grain boundary (CSL or general), p is the length fraction of the grain boundary covered by precipitates of type i (Cr-rich or Mo-rich), $B_{b,p,i}$ is the number of boundaries of type b with length fraction p of precipitates of type i, and N_b is the total number of grain boundaries of type b within the specimen that contained precipitates. Low-angle grain boundaries were omitted from this analysis because few boundaries were low-angle and only a small fraction of those had precipitates on them. In the interest of space, the findings are shown in Figure 7 for a few representative specimens where the number fraction of grain boundaries is plotted versus the length fraction of the grain boundary covered by precipitates; the length fractions were divided into 0.1 increments from 0 to 1. The plots are differentiated by both the type of precipitates (Cr- or Mo-rich in the left and right columns, respectively) and by the specimen conditions. The data are plotted as a cumulative distribution function (CDF) which illustrates whether a given type of grain boundary exhibited a higher degree of coverage by precipitates. For all specimens (including those not shown in the plot), the frequency of special

boundaries with a length fraction of coverage near zero is higher than that for the general grain boundaries. This is shown by the CDF for the special boundaries (gray line) being shifted toward zero as compared to that of the general boundaries (black line). This implies that the Σ3 boundaries exhibit a smaller fraction of boundary coverage than the general grain boundaries, or, in other words, the general grain boundaries were more heavily decorated with precipitates. These results are consistent with those in Figure 6.

4. Discussion

4.1. Grain Size and Grain Boundary Character Distribution

Analysis of the grain size distribution showed that almost no measurable grain growth occurred, even in the creep-deformed specimens, after up to 25 days at 1000°C. Given that the solutionizing temperature for this alloy is 1175°C, it is not unusual that little grain growth occurred. In addition, while precipitate redistribution to boundaries in tension is believed to occur, this is not accompanied by a shift in grain size which would be expected as boundaries become unpinned and are free to migrate. Therefore, while the redistribution can be quantified, its effects on the subsequent microstructural evolution and creep deformation are not observed here. However, it is important to note that these tests were not run to rupture, but for prescribed times or to predetermined strain levels.

Unlike the grain size distribution, the special boundary fraction does evolve during high temperature exposure. Specimens tested at 1000°C show a slight increase in the special boundary fraction as compared to those tested at 900°C and the as-received material. However, no consistent differences were observed between the special boundary fractions of the creep deformed and annealed sections, and thus we conclude that the addition of an applied stress does not lead to changes in grain boundary character. These results can be compared to those in Refs. [23, 27] where the microstructures of alloys 617 and 718 were found to remain relatively constant during either annealing or creep deformation. The stability of the special boundary fraction in those studies may be attributed to grain boundary pinning by the secondary phase precipitates, which inhibit grain boundary motion and improve microstructural stability in the creep-tested alloys. However, in the present work, we find that the special boundary fraction does evolve slightly during high temperature exposure. It is possible that the increase in special boundary fraction can be attributed to the increased population of precipitates on general boundaries as shown in Figures 6 and 7. In this case, the special boundaries, which typically are thought to have lower mobilities than general boundaries, are denuded of carbides and are more free to migrate, thus increasing their total length and the overall fraction of special boundaries without causing a significant increase in grain size.

4.3. Carbide Precipitate Analysis

The carbide precipitate distribution was initially determined with respect to the location and type of carbides. With a few exceptions, most specimens exhibited a higher fraction of precipitates on the grain boundaries than within the grains. Also, for many of the tests, the creep deformed specimen showed a larger fraction of precipitates on the grain boundaries as compared to the corresponding annealed specimens. This agrees with Ref. [2] where, during creep, the

intragranular carbides appeared to dissolve and re-precipitate as grain boundary carbides. In addition, He *et al.* performed creep tests at 800°C on the Ni-based superalloy M963 and determined that the precipitation of the Cr-rich phase on grain boundaries depended on both stress and temperature.[12] Precipitation was accelerated by the tensile stress and an optimal temperature existed for nucleation and growth of the secondary phase. A similar phenomenon is believed to have occurred in this study, where the higher applied stresses provided a stronger driving force for re-precipitation of the carbide phases.

Further inspection of Figure 3 shows that the higher fraction of grain boundary precipitates was primarily due an increase in the number of Mo-rich carbides on the grain boundaries in the creep-deformed areas. The fraction of Cr-rich precipitates on the grain boundaries did not show the same systematic increase from grip to gauge sections that the Mo-rich precipitates experienced. This implies that the creep conditions provided more favorable conditions for the dissolution and re-precipitation of the Mo-rich precipitates. Although the number of precipitates analyzed in the present study may not be considered statistically extensive, the consistent increase in the fraction of Mo-rich carbides on the grain boundaries from grip to gauge sections found for most specimens, especially those tested at 900°C, suggests that the phenomenon is real.

4.4. The Effect of Triple Junction Distribution on Carbide Precipitate Distribution

Figure 4 showed that triple junctions are predominately populated by Mo-rich carbides and that while J_0 and J_2 junctions have higher precipitate populations, J_3 junctions tend to be decorated by very few precipitates. One explanation for the increased population of Mo-rich carbides at the triple junctions is that the larger Mo atoms might have a lower solubility in the matrix than the Cr atoms do, driving them to the boundaries and ultimately to re-form precipitates at the triple junctions. Triple junction character (i.e., the number of special boundaries at the junction) and the presence of applied stress are also found to impact the distribution of precipitates at the junctions. When considering all specimens in this study, J_2 triple junctions very often have higher populations of carbides than do J_1 and J_3 junctions. A mechanistic explanation is related to the idea that Mo and Cr atoms should diffuse more easily along general grain boundaries. As diffusing atoms encounter a triple junction, they can either continue moving along a general boundary or cease to diffuse along grain boundaries if no easy diffusion paths exist. Accordingly, the probability of finding a J_2 triple junction (i.e., one general boundary and two special boundaries) with a precipitate should be high because the two special boundaries impede the continued diffusion of these atoms. This conceptual model also explains the low population of carbides at J_3 triple junctions; when all three boundaries are special (low diffusivity paths), the Mo and Cr atoms will be less likely to diffuse to those points resulting in fewer precipitates. At J_0 junctions where all three boundaries are general, diffusion to and from the junction is possible. Therefore, the relative decrease in precipitates at J_0 junctions in the presence of applied stress suggests that the diffusion may be biased to shift precipitates to other triple junction types. Finally, it is important to note that boundary character at the triple junction is not the sole influence on migration of carbide species; the angle between the boundary trace and applied stress axis can still bias the diffusion and re-precipitation of carbides.

4.5. The Effect of Grain Boundary Trace-Angle on Carbide Precipitate Distribution

In alloy 617 that has been exposed to creep conditions, carbide precipitates have been shown to redistribute to grain boundaries in tension.[2] Although this phenomenon was first observed decades ago, no quantitative analysis had yet been performed. We present here what is, to the best of the authors' knowledge, the first quantitative study of precipitate redistribution and consider also the effects of applied stress and temperature on the resulting redistribution. As Figure 5 shows, the precipitate distribution with respect to the boundary trace-angle relative to the stress axis can be determined and comparisons drawn between areas with and without applied stress. As in Ref. [2], we find evidence that grain boundaries in tension (i.e., those normal to the stress axis) are more heavily decorated with precipitates than those parallel to the stress axis. Furthermore, a more systematic shift of Cr-rich precipitates to grain boundaries is tension is observed in the present work (black bars in Fig. 6). These finding agree with the results of Kihara *et al.*[2] who showed that the majority of the grain boundary precipitates were Cr-rich. In their work, the result is attributed to the higher diffusivity of Cr versus Mo in nickel-based alloys and the resistance of Mo-rich carbides to dissolution as compared to Cr-rich carbides.

A few conclusions emerge from the present study. First, the area analyzed for precipitate redistribution must be sufficiently large in order to include enough boundaries and precipitates to observe the effect. As Figure 1 shows, the trend is obvious at a large scale, but analysis of only a fraction of the area shown in Figure 1 might not quantitatively show the redistribution. Second, analysis of a small area (e.g., corresponding the top right plot in Figure 5) can show an extremely high fraction of boundaries with precipitates. In contrast, the large scan areas that correspond to the lower three rows of Figure 5 show a relatively constant fraction of boundaries decorated by precipitates. Future analyses like the present one should use areas with sufficient size to avoid what might be artifacts of the scan area and to establish a minimum analysis area which can reliably show microstructural differences. Precipitate distributions that are quantitatively distinct can then be linked to the properties of interest to determine how significant a role the microstructure plays in affecting the properties. Finally, our data suggest that the applied stress plays a role in the degree of precipitate redistribution indicating that the diffusion of Mo and Cr atoms is stress-assisted. In this case, high applied stresses would lead to more evidence of redistribution, an effect that is observed throughout our analysis.

4.6. The Effect of Grain Boundary Character on Carbide Precipitate Distribution

In addition to the grain boundary trace-angle relative to the stress access, the grain boundary character affected the carbide precipitate redistribution (Figures 6 and 7). Specifically, precipitates were less likely to be found on CSL boundaries (which are primarily $\Sigma 3$ twin boundaries) than general boundaries, and CSL boundaries contained a lower fraction of coverage by the precipitates than did the general grain boundaries. These results are intuitive based on the structures and relative interfacial energies of the two types of grain boundaries. The higher-energy general boundaries have a more open structure with low atomic matching, while the CSL boundaries are more likely to be low-energy and have a higher degree of atomic matching. In addition, Figure 6 shows that at 1000°C a higher stress tended to promote a more pronounced shift in precipitates onto general boundaries. As our other analyses have shown, this suggests

that stress-assisted diffusion is occurring and a shift to general boundaries from special boundaries would be expected.

The findings of the present work can be compared to previous studies which considered the effect of grain boundary character on precipitate distribution (although not on redistribution during creep testing). Liu *et al.* found that carbides on low-Σ CSL boundaries tended to be smaller than the carbides found on the general grain boundaries.[5] Here, we also find that precipitation of the intergranular carbides is suppressed on low-Σ CSL boundaries, as compared to the general high-angle boundaries (Figures 6 and 7). This suppression is likely due to the relative grain boundary energies as suggested by others.[4, 5] Lim *et al.* studied the effect of boundary misorientation on Cr-rich $M_{23}C_6$ precipitates in alloy 690 and found that general grain boundaries were decorated with coarse and irregular carbides and that Σ3 coherent twins were devoid of any carbides.[4] While we find that general boundaries contain more precipitates than do special boundaries, we still find a relatively high fraction of precipitates on the special boundaries. This necessarily includes precipitates on Σ3 boundaries since they make up the vast majority of special boundaries. It must be noted, however, that the analysis in Ref. [4] was performed with TEM (and its resolution limits) while the present study was focused on the larger precipitates that can be observed with SEM. Therefore, it is possible that the evolution of the finest scale carbide precipitates occurs differently than that of the macroscale precipitates.

4.7. Mechanism of Precipitate Evolution

Finally, it is important to consider whether the evolution of the precipitate distribution is due to the precipitates migrating onto essentially stationary boundaries or precipitate-free grain boundaries migrating until they encounter precipitates. The first mechanism would involve the dissolution of precipitate phases, the diffusion of precipitate species, and the re-precipitation of carbides at grain boundaries. The second mechanism would require the migration of un-pinned boundaries (those free of precipitates) until their motion was impeded by a carbide particle. Based on the results of the present work and of previous work by others,[2, 10] we believe that redistribution occurs by the dissolution, diffusion (along grain boundaries and/or through grain interiors) and re-precipitation of the carbides on the grain boundaries. This mechanism is consistent with the distribution of precipitates at grain boundary triple junctions in stressed and unstressed specimens (Figure 4) where grain boundary character plays a role in the redistribution process as diffusion along the boundaries occurs. Were stress-assisted grain boundary migration to occur, the distribution of grain boundary trace angles (when considering all boundaries) would be expected to change; no such change is observed here. In addition, if the boundary migration mechanism were taking place, the creep deformed specimens should show some boundary bowing as a result of migration and subsequent pinning. While this phenomenon has been observed in some specimens tested to higher strains than those presented here, no evidence of changes to the microstructural topology are realized between annealed and creep deformed specimens in the present study, so this mechanism is unlikely. Finally, the absence of significant grain growth or changes to the grain aspect ratios at these test temperatures and stresses suggests that there is not extensive boundary migration by boundaries with or without precipitates.

5. Conclusions

The goal of the present study was to quantify the effects of both grain boundary character and grain boundary trace-angle on the redistribution of Cr- and Mo-rich precipitates in alloy 617 during creep deformation at 900 and 1000°C. Specifically, we sought to understand the effects of temperature and applied stress on the evolution of the precipitate distribution. As the carbide precipitates provide high temperature strength to the material, understanding how they evolve during creep deformation is important in order to predict the behavior of these materials in other operating conditions. The following are the main conclusions of this investigation:

- Quantitative metrics were developed which allow for analysis of precipitate distribution with respect to precipitate type, grain boundary character and the angle between the grain boundary trace and applied stress axis.

- Mo-rich precipitates were shown to be more prevalent at triple junctions than were Cr-rich precipitates. Among triple junction types, J_2 triple junctions (i.e., those with two special boundaries) were more likely than J_1 or J_3 junctions to be populated by precipitates. We suggest that this is related to the higher diffusivity of general high-angle boundaries.

- The precipitation of intergranular carbides is suppressed on low-Σ CSL boundaries as compared to general high-angle boundaries. Not only are precipitates more likely to occupy general boundaries, the general boundaries are more likely to have a higher length fraction of precipitate coverage than are special boundaries.

- The quantitative analysis developed here is capable of resolving changes in the precipitate distribution with respect to the angle between the grain boundary trace and the stress axis. Higher applied stresses during creep lead to a more pronounced shift in precipitate distribution toward the boundaries in tension.

- Our results indicate that the applied stress of creep testing plays an important role in the subsequent diffusion of Mo and Cr atoms and leads to the observed evolution of the precipitate distribution.

Acknowledgements

This work was supported by the Idaho National Laboratory. The Boise State University authors were also supported in part by the Center for Advanced Energy Studies (Idaho Falls, ID) and the Department of Energy.

REFERENCES

1. H.J. Christ, U. Kunecke, K. Meyer, H.G. Sockel: *Mater. Sci. Eng.*, 1987, vol. 87, pp. 161-68.
2. S. Kihara, A. Ohtomo, Y. Saiga, J.B. Newkirk: *Metall. Mater. Trans. A*, 1980, vol. 11A, pp. 1019-31.
3. F. Jalilian, M. Jahazi, R.A.L. Drew: *Materials Science and Engineering: A*, 2006, vol. 423, pp. 269-81.
4. Y.S. Lim, J.S. Kim, H.P. Kim, H.D. Cho: *Journal of Nuclear Materials*, 2004, vol. 335, pp. 108-14.
5. H. Liu, M. Gao, D.G. Harlow, R.P. Wei: *Scripta Metallurgica et Materialia*, 1995, vol. 32, pp. 1807-12.
6. K. Mino, A. Ohtomo: *Transactions of the Iron and Steel Institute of Japan*, 1978, vol. 18, pp. 731-38.
7. K. Bhanu Sankara Rao, H.P. Meurer, H. Schuster: *Materials Science and Engineering A*, 1988, vol. 104, pp. 37-51.
8. W.L. Mankins, J.C. Hosier, T.H. Bassford: *Metall. Mater. Trans. A*, 1974, vol. 5, pp. 2579-90.
9. J. Schwertel, K. Hornberger, B. Schinke, G. Merckling, D. Munz. Proceedings of the ASME Conference on Materials. 1991, vol. 26, pp. 285-95.
10. G.D. Smith, D.H. Yates. Proceedings of the International Gas Turbine and Aeroengine Congress and Exposition. 1991, vol. pp. 5-12.
11. Q.Y. Wu, H.J. Song, R.W. Swindeman, J.P. Shingledecker, V.K. Vasudevan: *Metall. Mater. Trans. A*, 2008, vol. 39A, pp. 2569-85.
12. L.Z. He, Q. Zheng, X.F. Sun, G.C. Hou, H.R. Guan, Z.Q. Hu: *Journal of Materials Science*, 2005, vol. 40, pp. 2959-64.
13. G. Palumbo, K.T. Aust, E.M. Lehockey, U. Erb, P. Lin: *Scripta Materialia*, 1998, vol. 38, pp. 1685-90.
14. V. Randle: *Materials Characterization*, 2001, vol. 47, pp. 411-16.
15. C.A. Schuh, M. Kumar, W.E. King: *Journal of Materials Science*, 2005, vol. 40, pp. 847-52.
16. W.D. Callister Jr: *Materials Science and Engineering An Introduction*, John Wiley & Sons, Inc.,New York, 2003.
17. K. Barmak, J. Kim, C.S. Kim, W.E. Archibald, G.S. Rohrer, A.D. Rollett, D. Kinderlehrer, S. Ta'asan, H. Zhang, D.J. Srolovitz: *Scripta Materialia*, 2006, vol. 54, pp. 1059-63.
18. G.S. Rohrer: *Structure and Bonding in Crystalline Materials*, Cambridge University Press,Cambridge, UK, 2001.
19. H.U. Hong, B.S. Rho, S.W. Nam: *Mater. Sci. Eng.*, 2001, vol. 318, pp. 285-92.
20. B.Q. Li, A.P. Reynolds: *J. Mater. Sci.*, 1998, vol. 33, pp. 5849-53.
21. E.M. Lehockey, G. Palumbo: *Materials Science and Engineering A*, 1997, vol. 237, pp. 168-72.
22. C.J. Boehlert, D.S. Dickmann, N.C. Eisinger: *Metallurgical and Materials Transactions A*, 2006, vol. 37A, pp. 27-40.

23. L. Tan, K. Sridharan, T.R. Allen, R.K. Nanstad, D.A. McClintock: *Journal of Nuclear Materials*, 2008, vol. 374, pp. 270-80.
24. L. Tan, K. Sridharan, T.R. Allen: *Journal of Nuclear Materials*, 2007, vol. 371, pp. 171-75.
25. T.M. Lillo, J. Cole, M. Frary, S.M. Schlegel: *Metall. Mater. Trans. A*, 2009, vol., pp.
26. D.G. Brandon: *Acta Metallurgica*, 1966, vol. 14, pp. 1479-84.
27. C.J. Boehlert, D.S. Dickmann, N.C. Eisinger: *Metall. Mater. Trans. A*, 2006, vol. 37A, pp. 27-40.

TABLES

Table 1. Composition of alloy 617 (amounts are in wt %).

C	Mn	Fe	S	Si	Cu	Cr	Al	Ti	Co	Mo	B	Ni
0.08	0.11	1.69	<0.001	0.12	0.04	21.91	0.96	0.34	11.42	9.78	0.002	Bal.

Table 2. Creep test conditions.

Sample ID	Temperature (°C)	Time (h)	Stress (MPa)	Total Strain (%)
10	900	265	35	8.2
08	900	528	40.25	17.1
06A	1000	497	18.6	13.9
05-1	1000	617.6	19.8	29.4
06	1000	137	25	14.2
05-5	1000	170.2	26.8	23.5
05-4	1000	100.8	30.2	19.6

Table 3. Microstructural statistics for the annealed and creep deformed analysis areas.

Sample ID	Applied stress (MPa)	Scan area (10^3 μm^2)	Grain size (μm)	HA boundary fraction	LA boundary fraction	CSL boundary fraction	Number of PPTs	Number of GBs
AR	n/a	122.5	12	0.42	0.02	0.56	39	400
10	0	90	8.9	0.4	0.02	0.58	69	354
10	35	32.4	5	0.39	0.05	0.56	637	633
08	0	32.4	5.7	0.5	0.03	0.47	377	220
08	40.25	16.2	4.7	0.56	0.01	0.43	125	371
06A	0	192	11.7	0.33	0.02	0.65	137	244
06A	18.6	32.4	5.2	0.44	0.03	0.53	234	575
05-1	0	200	14.1	0.2	0.06	0.74	286	636
05-1	19.8	270	12.4	0.28	0.07	0.64	266	955
06	0	50	4.4	0.44	0.06	0.5	122	270
06	25	27	5.2	0.4	0.05	0.55	88	250
05-5	0	308.75	14.1	0.3	0.06	0.64	303	1092
05-5	26.8	308.75	12.3	0.27	0.09	0.64	376	1340
05-4	0	247.5	12.0	0.26	0.06	0.68	295	1137
05-4	30	247.5	13.3	0.31	0.05	0.63	187	1001

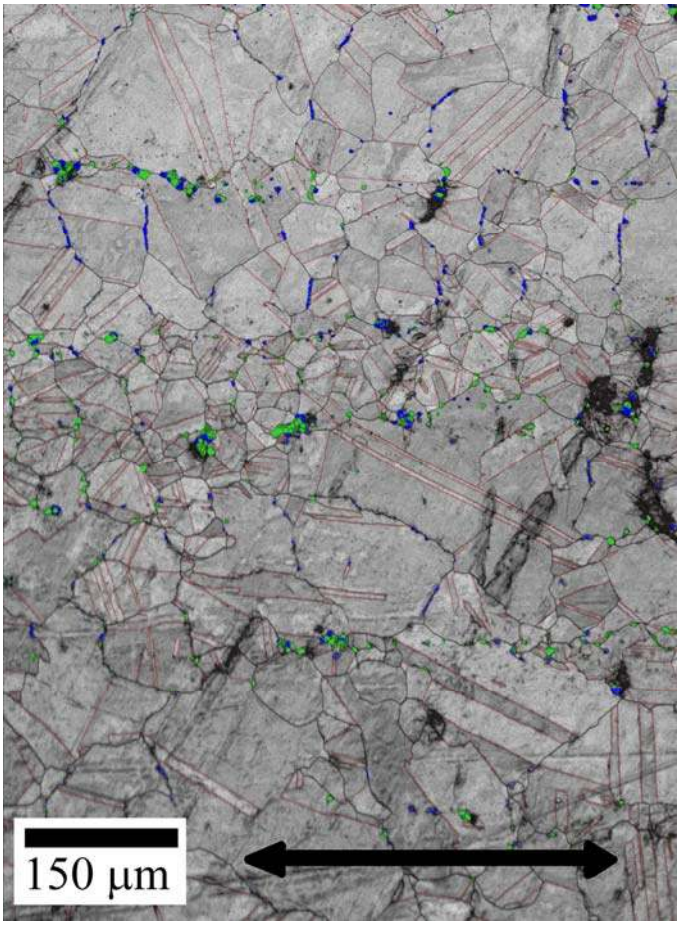

Figure 1: Microstructural map from the specimen tested at 1000°C and 19.8 MPa showing grain boundary character (red lines are CSL boundaries, black lines are general high-angle boundaries) and precipitate location (blue and green regions indicate high Cr and Mo concentrations, respectively). The arrow indicates the direction of applied stress during the creep test.

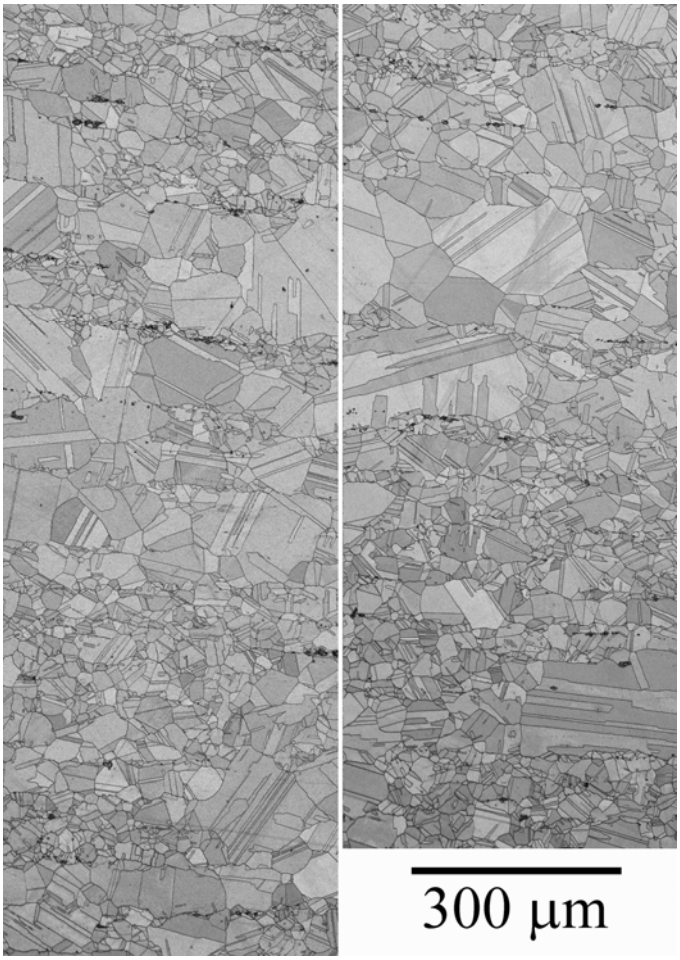

Figure 2: Microstructure of the as-received alloy 617. The horizontal direction in the picture is parallel to the specimen axis.

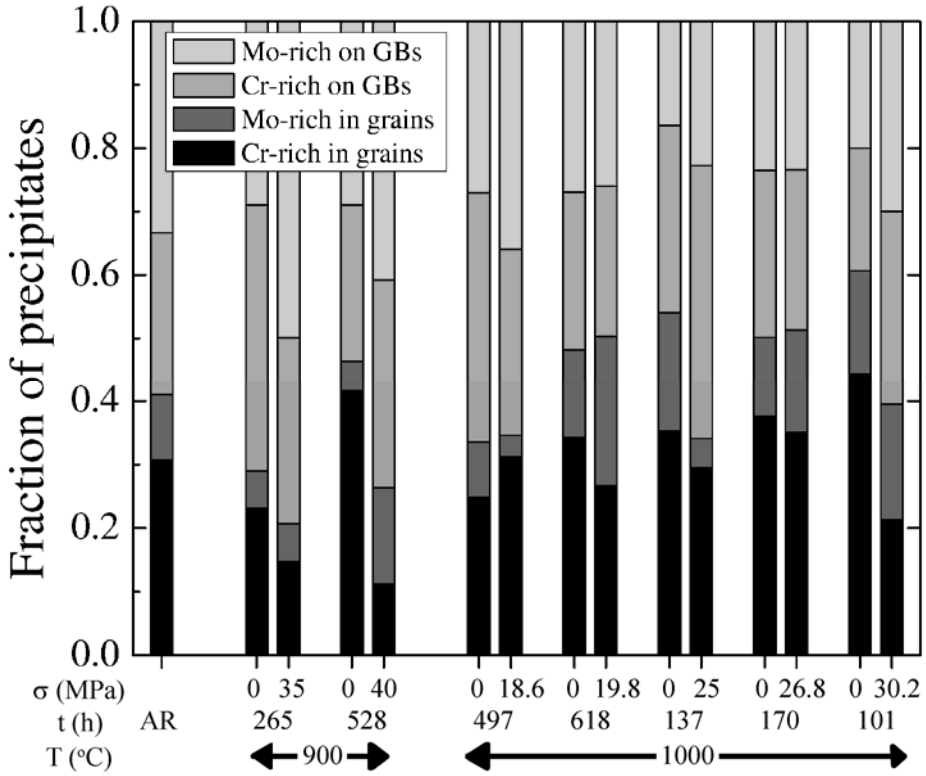

Figure 3: Distribution of Cr- and Mo-rich carbides by location (in grains or on grain boundaries). Each column corresponds to a different specimen (as-received, annealed or creep deformed) as given by the conditions below the figure.

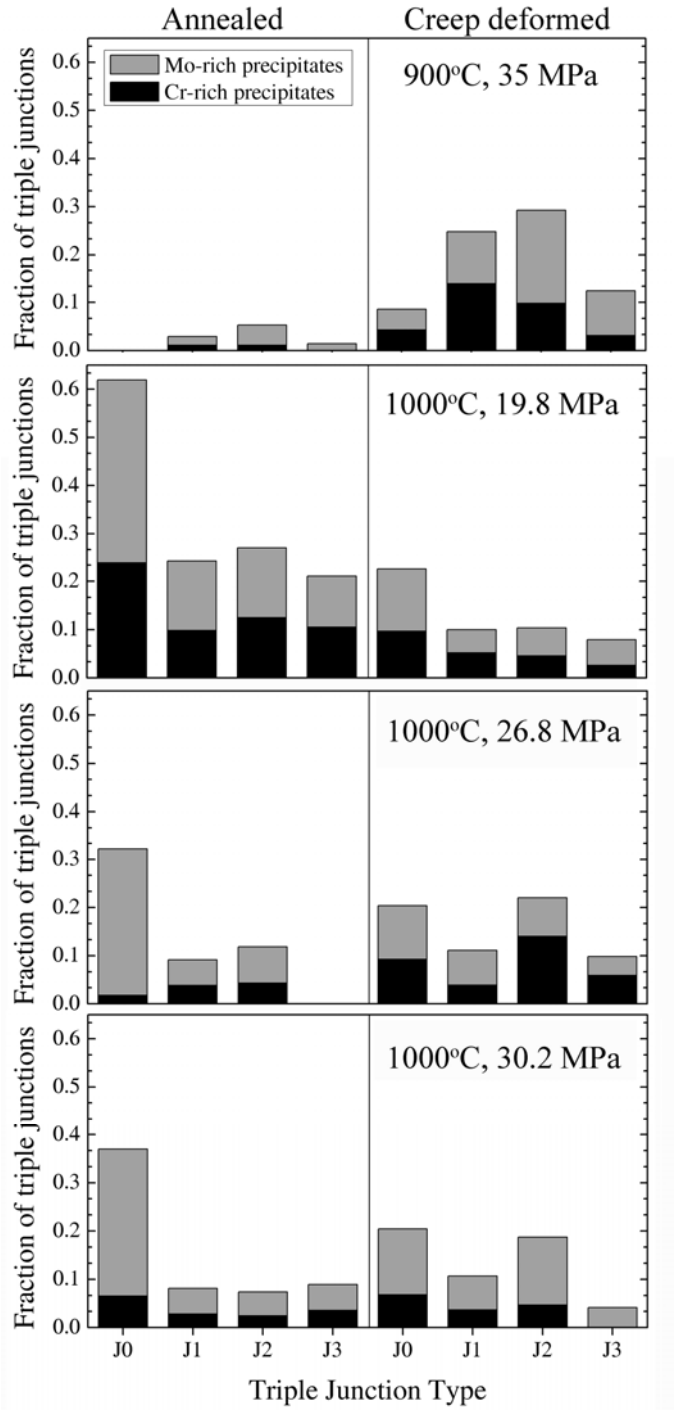

Figure 4: The fraction of triple junctions with carbide precipitates, $T(i,j)$, for annealed (left column) and creep deformed (right column) specimens under different test conditions.

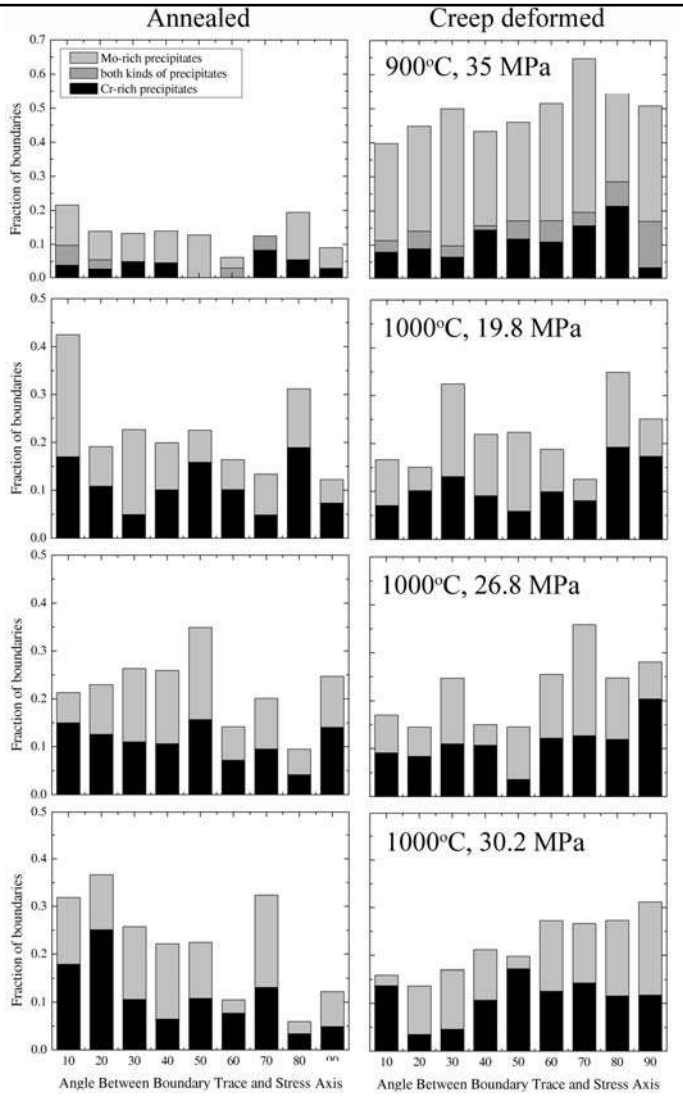

Figure 5: The distribution of grain boundaries with precipitates, $f(i,\theta)$ differentiated by the grain boundary trace-angle relative to the stress axis, where 0° corresponds to a boundary aligned parallel to the stress, for annealed (left column) and creep deformed (right column) specimens under different test conditions.

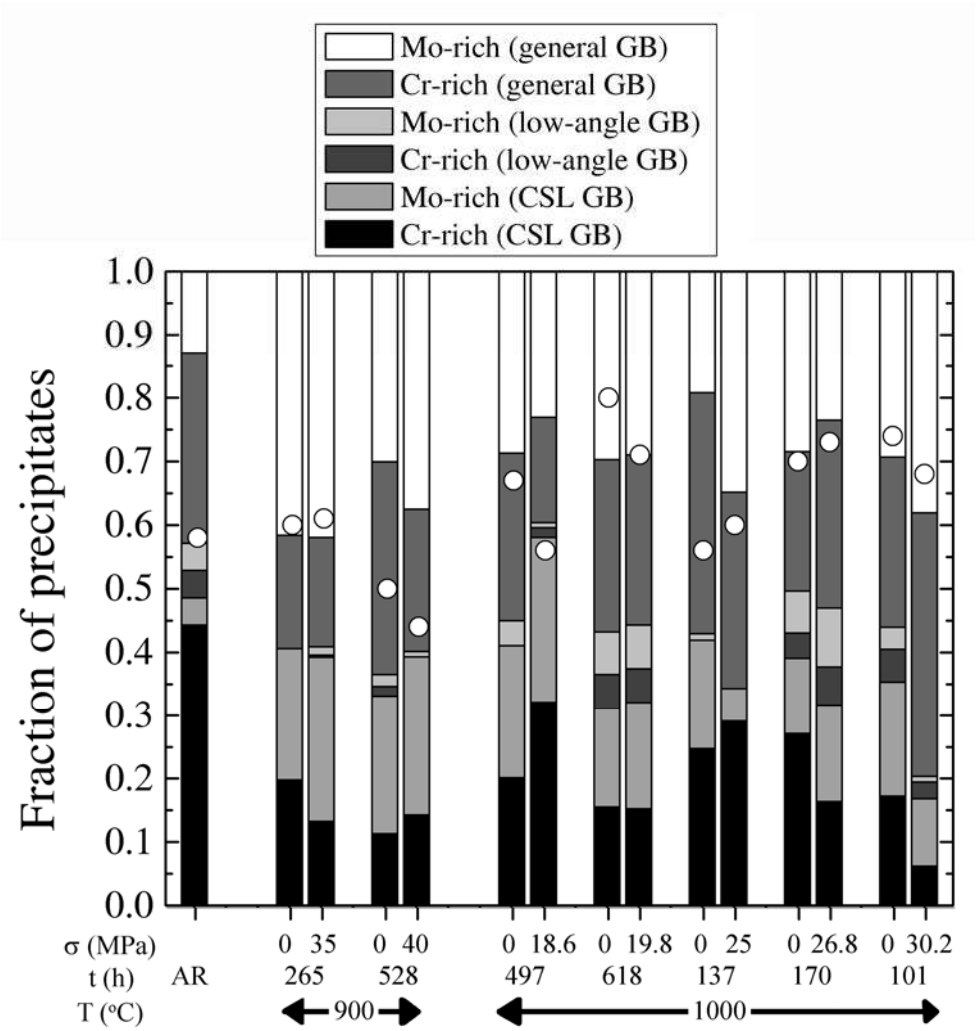

Figure 6: Distribution of Cr- and Mo-rich carbides by grain boundary type (general, low-angle, or CSL), *y(i,b)*. Each column corresponds to a different specimen (as-received, annealed or creep deformed) as given by the conditions below the figure. From the top to the bottom of the column, the areas represent Mo-rich precipitates on general boundaries, Cr-rich precipitates on general boundaries, Mo-rich precipitates on low-angle boundaries, Cr-rich precipitates on low-angle boundaries, Mo-rich precipitates on CSL boundaries, and Cr-rich precipitates on CSL boundaries. The white dot represents the total fraction of grain boundaries that are low-angle or CSL boundaries.

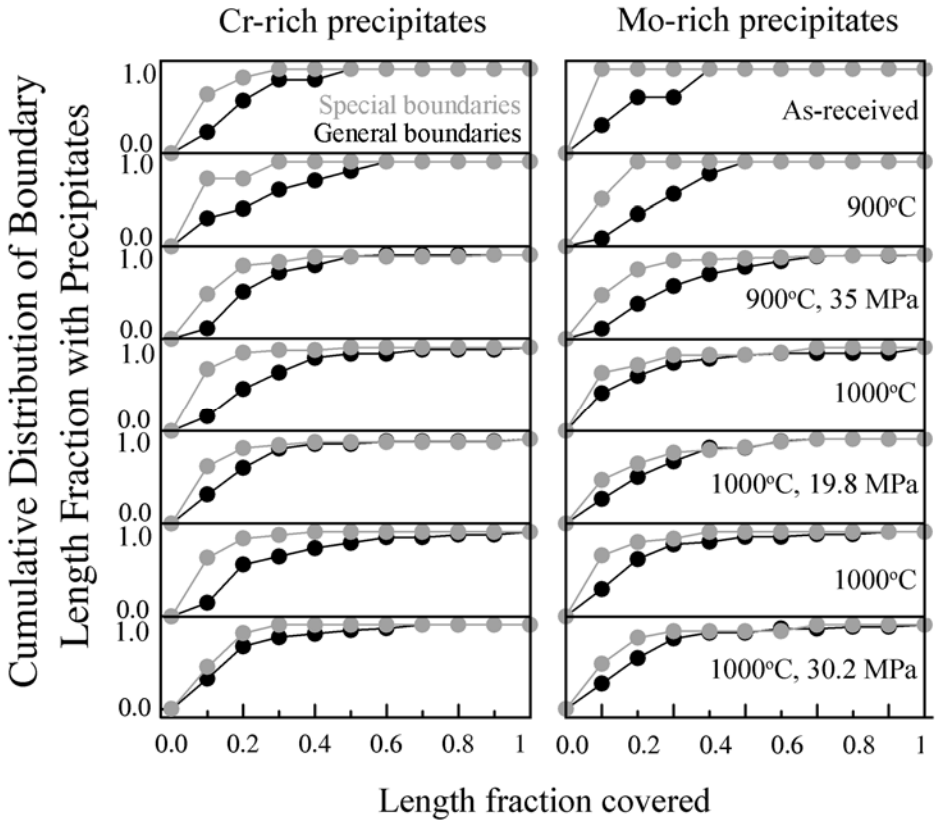

Figure 7: The distribution of grain boundaries based on the length fraction of precipitate coverage, *g(b, p, i)*, for Cr-rich (left column) and Mo-rich (right column) precipitates under different test conditions. The gray points and lines represent the special boundaries, the black points and lines the general boundaries.